PHYSICAL REVIEW B **89**, 121409(R) (2014)

# Electronic surface potential from angle-resolved photoemission

G. Vasseur,* Y. Fagot-Revurat, B. Kierren, M. Sicot, and D. Malterre
*Université de Lorraine, Institut Jean Lamour, UMR 7198, Boîte Postale 70239, 54506 Vandœuvre-lès-Nancy, France*
(Received 11 September 2013; published 20 March 2014)

We present a methodology to determine the periodic potential of a surface from angle-resolved photoemission spectroscopy. By mapping the band structure and measuring the energy gap widths at high symmetry points of the surface Brillouin zone, the first Fourier components of the potential can be estimated. This method has been applied in the case of the reconstructed Ag/Cu(111) surface where controlled potassium atom doping has been used to precisely tune the band gap energies. This potential determination allows one to calculate the local density of states which is found to be in very good agreement with scanning tunneling spectroscopy data.

DOI: 10.1103/PhysRevB.89.121409 PACS number(s): 73.20.At, 73.22.−f, 79.60.−i

Band structures of solids reflect the potential probed by the electrons. This electronic potential is usually only obtained from *ab initio* calculations in density functional theory approach and the corresponding band structures may be compared with experiments using essentially angle-resolved photoemission spectroscopy (ARPES). An approach was proposed to map the surface electronic potential from scanning tunneling microscopy (STM) by using the linear response theory [1]. We will show that it is possible to directly obtain the potential from ARPES experiments. This method is based on the measurement of band gaps at the high-symmetry points of the Brillouin zone (BZ) which allow the determination of Fourier components of the potential.

Let us recall some information about the relation between band structure and symmetry. The band degeneracy, especially at the high-symmetry points, is a direct consequence of the potential symmetry and more precisely of the symmetry of the wave vector group at the considered BZ point [2]. The wave vector group is the group of operations leaving the wave vector unchanged. A change of degeneracy or of the dispersion relation can result from a symmetry breaking (change of the wave vector group). For example, in graphene the Dirac points with their twofold degeneracy and the linear dispersion near the $K$ points correspond to the two-dimensional (2D) irreducible representation of the $C_{3v}$ wave vector group. A symmetry breaking which changes the wave vector group at the $K$ point, achieved by putting a graphene layer on an appropriate substrate, leads to a gap opening and then to massive fermions [3,4].

Such a gap opening can be studied in reconstructed nanostructurated lattices at the surface of (111) noble metals. Surface Shockley states develop on these (111) surfaces with nearly-free-electron-like behavior [5]. Therefore parabolic dispersions are observed with deviations close to the surface BZ boundary. For example, confinement and/or gap openings have been observed for vicinal surfaces due to the one-dimensional periodic potential corresponding to the step array [6]. In Au vicinal surfaces, additional superperiodicity parallel to the steps exists due to the herringbone reconstruction of the Au(111) surface on terraces leading to very small gaps [7]. Another famous example is the Ag/Cu(111) interface where an hexagonal array of triangular dislocations was observed [8,9]. The corresponding $\sim(9.5 \times 9.5)$ superperiodicity induces the opening of gaps observed at the $M$ point of the surface BZ of the reconstruction [10–12].

Due to the plane wave character of the Shockley state, the gap opening results from the Bragg mechanism at the BZ boundaries and their magnitudes are simply related to the corresponding Fourier components ($V_{\vec{G}}$) of the potential in the first approximation of perturbation theory. At the $M$ point of the hexagonal surface BZ, the gap magnitude is simply $2|V_{\vec{G}}|$-like in a simple 1D nearly-free-electron gas discussed in solid state textbooks [13]. Therefore the gap width only gives partial information (the modulus) about the potential. It has been shown by combining ARPES and scanning tunneling spectroscopy (STS) that both the magnitude and the phase of the first Fourier components of the Au reconstruction on a Au vicinal surface can be obtained [7]. In this Rapid Communication, we would like to show that a detailed description of the potential can be achieved by measuring the gaps at the different high-symmetry points ($\Gamma$, $M$, and $K$) and directions. However, only the first low energy gap corresponding to occupied states can be probed by ARPES in Ag/Cu(111). The technical key point of the present work is to use controlled potassium doping to precisely tune the energy position of the band gaps since K adsorption changes the work function and shifts down in energy the Shockley state [14,15]. By using different K doping, we succeeded in measuring quantitatively several gaps in the different directions of the Brillouin zone and we obtained a complete determination of the Shockley band structure. The gap values at several high-symmetry points allow one to determine not only the norm but also the real and imaginary parts of the first Fourier components of the potential. It gives a satisfactory description of this potential since the calculated local density of states is found to be in very good agreement with local spectroscopic properties probed by STS. This demonstrates the interest and strength of this original methodology in estimating the surface potential.

The angle-resolved photoemission experiments were performed at 80 K with a Scienta 200 high-resolution hemispherical analyzer using a photon energy of $h\nu = 21.2$ eV. Data points in Fig. 2 are obtained from standard line fits of individual energy distribution curves (EDCs), using Lorentzian functions and Fermi edge functions. Features that lie within $\pm 2k_BT$

*Corresponding author: guillaume.vasseur@univ-lorraine.fr

 

of $E_F$ are cut off by the Fermi edge. Peaks above $E_F$ can thus be visualized by normalizing the EDCSs with the Fermi-Dirac distribution function convoluted with the experimental resolution. STM and STS experiments have been carried out using an Omicron STM. The $dI/dV$ spectra and maps were recorded at 5 K in the open feedback loop mode using the lock-in technique with a bias modulation of 5 mV rms at 2300 Hz (stabilization parameters: set point 1 nA, bias 0.8 eV). Before transferring to the STM cryostat at 5 K, the Ag monolayer is evaporated at 150 K on the clean Cu(111) crystal, and then annealed to 350 K. This process leads to an $\sim(9.5 \times 9.5)$ hexagonal lattice of triangular dislocations. Evaporation of K atoms in the submonolayer range was achieved by heating a standard K getter. Band structure dispersions are computed by a direct diagonalization of the Schrödinger equation with a potential defined by the two first Fourier components in a plane wave basis limited to the first 36 waves around Γ. Note that additional plane waves have negligible effects. Local density of states (LDOS) maps and spectra are obtained resolving the Hamiltonian for more than 1500 wave vectors in the first BZ and by taking into account a 15-meV Gaussian energy broadening.

First of all, we will discuss angle-revolved photoemission spectroscopy measurements recorded along high-symmetry directions ($\Gamma M$ and $\Gamma K$) of the first BZ of the undoped and K-doped reconstructed Ag/Cu(111) surface. Figures 1(a) and 1(b) show the second derivative of the ARPES signal for a bare and a K-doped surface, respectively. These maps clearly show the parabolic dispersion of the Shockley surface state with energy gaps appearing at the boundary of the BZ. First, K deposition shifts the surface state energy at Γ by 300 meV towards higher binding energy. This behavior is well known and reflects the lowering of the work function with alkali metals [16,17]. This shift of the surface state is proportional to the amount of K atoms evaporated on the surface. Secondly, the surface state remains well defined and only a small broadening is induced by the K deposition. For the bare interface, an 80-meV gap opens below the Fermi energy ($E_F$) [10–12] at the $M$ point of the 2D BZ shown in Fig. 1(c) and although the gap at the $K$ point which is very close to the Fermi energy is not clearly resolved, the analysis of the spectral shape reveals that a small gap ($30 \pm 15$ meV) appears in agreement with previous measurements at room temperature [4]. In the K-doped surface, this gap is well below the Fermi energy and can be estimated more accurately, $E_{K_2} - E_{K_1} = 32 \pm 5$ meV [inset of Fig. 1(b)]. In addition, a band is emerging at $E_{K_3}$.

The characteristics of the energy spectrum at the high-symmetry points can be simply understood by considering the topology of the reciprocal space and the band energy calculated in the nearly-free-electron framework. Indeed, the gap widths depend on the Fourier components of the surface potential which can be decomposed:

$$V(\vec{r}) = \sum_{\vec{G}_n^{(p)}} V_{\vec{G}_n^{(p)}} e^{i\vec{G}_n^{(p)}\cdot\vec{r}}. \quad (1)$$

Symmetry gives us some relations between the different Fourier components. In the hexagonal reciprocal space lattice, one has six first neighboring points ($\vec{G}_n^{(1)}$ with $n = 1,2,\ldots,6$)

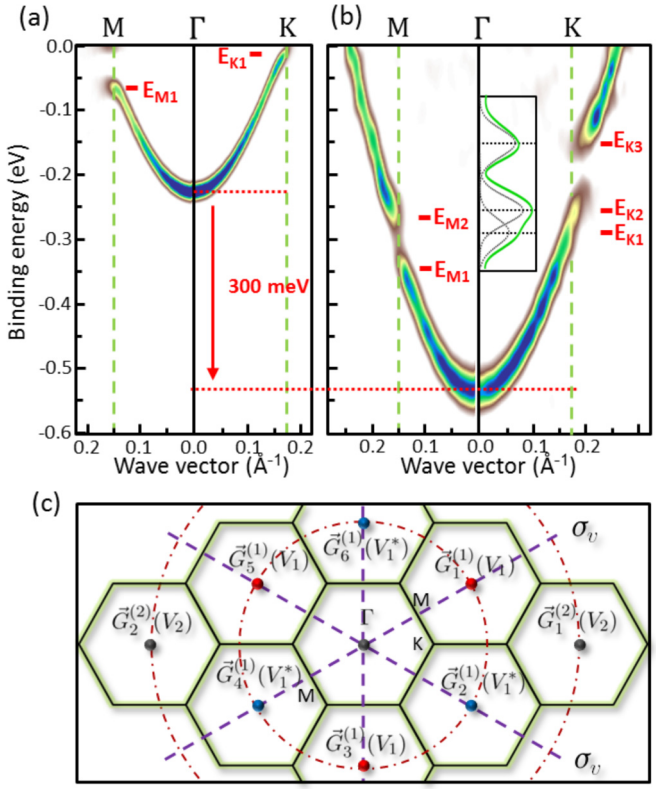


FIG. 1. (Color online) Experimental band dispersions (second derivative) of the Shockley state along the $\Gamma M$ and $\Gamma K$ directions for (a) the bare triangular reconstructed Ag/Cu(111) surface and (b) a K-doped surface (inset: energy cut very close to the $K$ point exhibiting the three eigenenergies). (c) Reciprocal space showing the high-symmetry points of the 2D BZ and the first neighboring reciprocal vectors. We also indicate the symmetry mirrors ($\sigma_v$) and the Fourier components of the potential associated with the reciprocal vectors in the first two rings around the Γ point (dashed circles).

around the central Γ point [first ring in dashed line in Fig. 1(c)]. However, these points are not equivalent since there is no sixfold symmetry axis and only a threefold one ($C_3$). Then only $\vec{G}_1^{(1)}$, $\vec{G}_3^{(1)}$, and $\vec{G}_5^{(1)}$ or $\vec{G}_2^{(1)}$, $\vec{G}_4^{(1)}$, and $\vec{G}_6^{(1)}$ are equivalent. As a consequence, two different Fourier components are associated with these two sets of $C_3$ equivalent vectors. However, time-reversal symmetry which transforms a wave vector in its opposite connects these inequivalent points. As a consequence, if $V_{\vec{G}}$ is the Fourier component for $\vec{G}$, then $V_{-\vec{G}} = V_{\vec{G}}^*$. In summary, the Fourier components in the first ring around Γ are $V_{\vec{G}_n^{(1)}} = V_1$ for $n = 1,3,5$ and $V_{\vec{G}_n^{(1)}} = V_1^*$ for $n = 2,4,6$.

Let us now investigate the effects of these Fourier components on the band energies at the $M$ and $K$ points in a very crude approximation. As the $M$ point is located in between two neighboring reciprocal vectors, $\vec{0}$ (Γ) and $\vec{G}_1^{(1)}$, there are two states associated with the plane waves originating from these two reciprocal vectors. The diagonalization of the corresponding $2 \times 2$ Hamiltonian leads to a gap width $\Delta E_M = E_{M_2} - E_{M_1} = 2|V_1|$. The $K$ point is located in the center of an equilateral triangle defined by three reciprocal nodes [Fig. 1(c)] and then three plane waves are involved and

the resolution of the 3×3 Hamiltonian leads to a gap width $\Delta E = E_{K_2} - E_{K_1} = 2\sqrt{3}\,\mathrm{Im}\,V_1$ and an excited state at $E_{K_3}$ ($E_{K_3} - E_{K_2} = 3\,\mathrm{Re}\,V_1 - \sqrt{3}\,\mathrm{Im}\,V_1$). These simple calculations show that the gap at the $K$ point is related to the imaginary part of $V_1$, so that $V_1$ can be completely obtained from ARPES measurements.

We can go further than this first approximation described above by extending the plane wave basis. We then consider 36 plane waves associated with 36 reciprocal vectors around Γ (additional vectors have nonsizable effects in the energy range corresponding to our spectroscopic measurements). We start from the $V_1$ value given by the analytical expressions above and we adjust it by using the extended basis in order to reproduce both the experimental energy gaps at $M$ and $K$ and the band dispersions in the high-symmetry directions. The energies have been determined by fitting the photoemission energy distribution curves for each $\vec{k}$ value by Lorentzian structures. The main intensity is found on the main parabola but small intensity is also observed on the folded bands. This method gives $V_1 = (47 + i9.6)$ meV.

The gaps involving the Fourier components associated with reciprocal vectors ($\vec{G}_n^{(2)}$) in the second ring are not accessible because they appear in unoccupied states. However, with increasing the amount of K adatoms, it is possible to shift the Shockley state in order to occupy states up to the second gap at the $M$ point. This is illustrated in the inset of Fig. 2 where a highly doped surface exhibits a gap opening of about 50 meV.

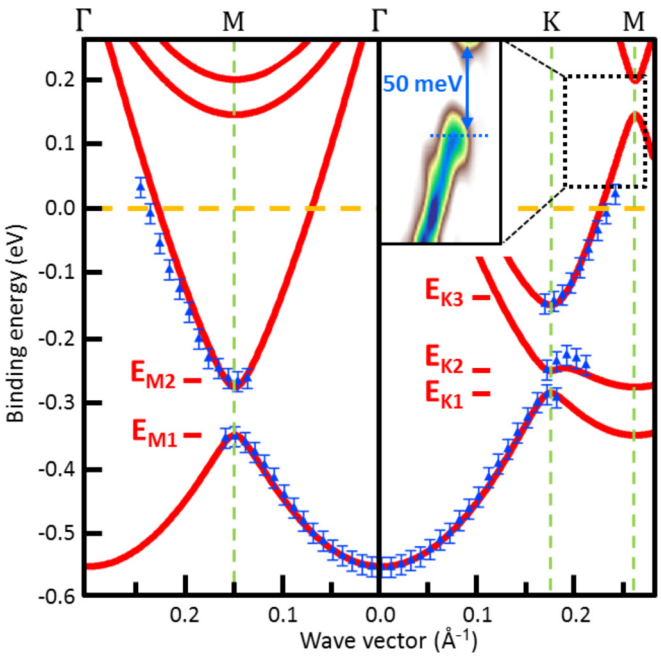


FIG. 2. (Color online) Band dispersion in the Γ$M$ and Γ$K$ directions determined from the K-doped surface of Fig. 1(b). Symbols are experimental values and the solid lines represent the calculated band structure obtained with a potential built from the Fourier components [$V_1 = (47 + i9.6)$ meV, $V_2 = 15$ meV] extracted from experimental gaps. Inset: experimental intensity of a highly K-doped surface illustrating the opening of a second gap at the $M$ point (see text).

The vertical mirror symmetry indicates that $V_{\vec{G}_2^{(2)}} = V_{\vec{G}_1^{(2)}} = V_2$ [Fig. 1(c)] demonstrating that the second Fourier component ($V_2$) is purely real. The magnitude of this gap depends on $V_2$ at first order and on $V_1$ at second order. The fitting method leads to a value of $V_2 \sim 15$ meV. It is worth mentioning that $V_2$ has a small effect on the dispersion and only affects the band structure close to this second gap at the $M$ point. The band dispersions along the high-symmetry directions Γ$M$ and Γ$K$ calculated with $V_1 = (47 + i9.6)$ meV and $V_2 = 15$ meV are shown in Fig. 2 (solid lines) and very good agreement with the experimental dispersions (symbols) is found. This surface potential directly deduced from experiments is one step beyond the potentials previously proposed to describe

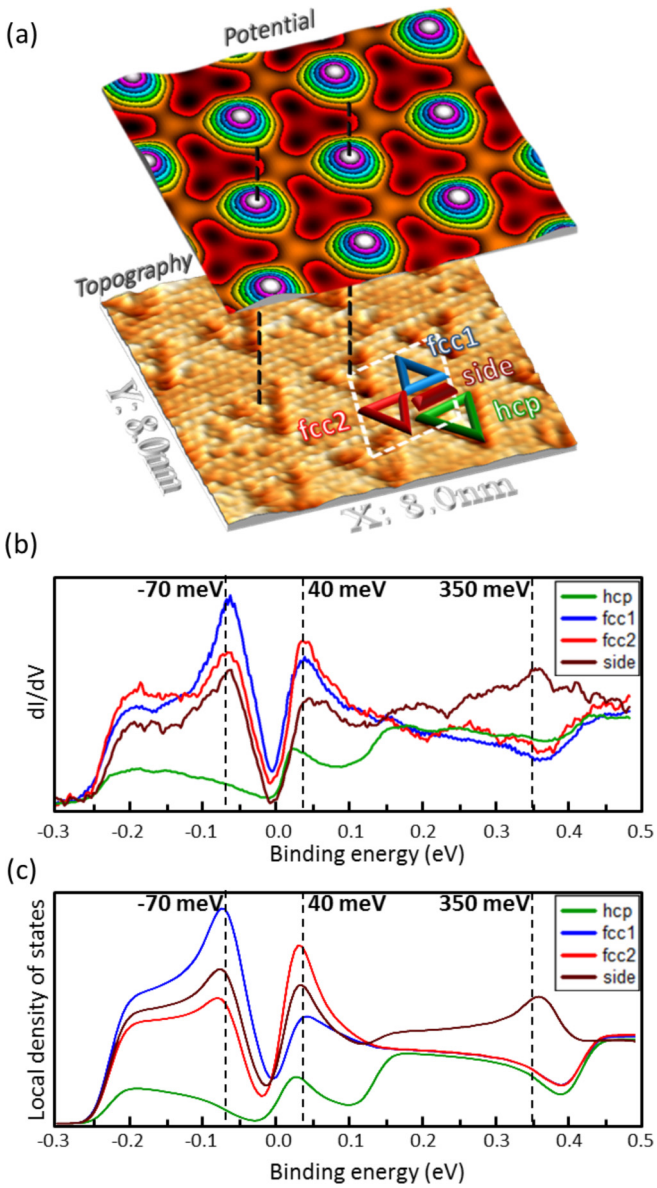


FIG. 3. (Color online) (a) Calculated potential and STM image corresponding to the same area showing the undoped reconstructed unit cell with the fcc1, fcc2, hcp, and side regions. Experimental $dI/dV$ spectra (b) and calculated LDOS (c) corresponding to the center of the different regions of the reconstructed unit cell.

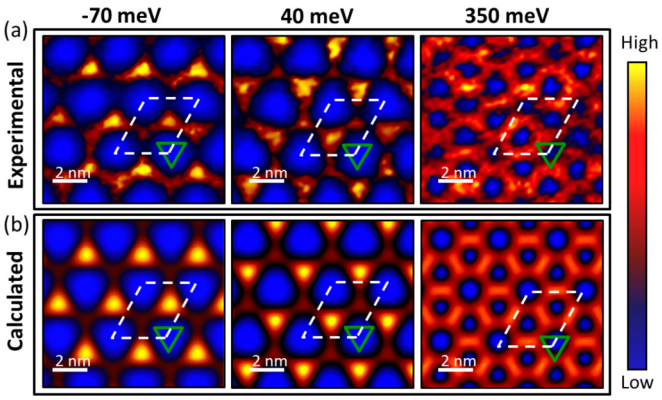


FIG. 4. (Color online) (a), (b) Experimental 2D $dI/dV$ maps and calculated LDOS corresponding to the bare Ag/Cu(111) surface at different energies (−70, 40, and 350 meV).

the Ag/Cu(111) surface [4,14]. In these papers, the shape of the surface potential was arbitrary postulated: It consists of areas with simple geometry (triangles and/or hexagons and are different in the two papers) corresponding to flat potentials whose values are free parameters adjusted in order to reproduce the experimental data.

Finally, in order to test the accuracy of the method, one can rebuild the 2D periodic potential and calculate local properties such as LDOS as a function of energy and position in the reconstructed supercell. By solving the Schrödinger equation with the determined surface potential, we obtain eigenfunctions $\Psi_{\vec{k}}(\vec{r})$ corresponding to a given energy $E$. The LDOS at position $\vec{r}$ and energy $E$ is calculated by summing $|\Psi_{\vec{k}}(\vec{r})|^2$ for all values of $\vec{k}$ in the first BZ. As the LDOS can be probed directly by STS, we will be able to give a quantitative comparison between calculations and spectroscopic measurements. The rebuilt 2D potential is plotted in Fig. 3(a) with a STM topographic image of the bare triangular reconstructed surface with the different regions characterized by their structural arrangement. We distinguish four areas: a triangular one corresponding to hexagonal compact packing (noted hcp), two face-centered-cubic packing (fcc1 and fcc2), and an intermediate region (side). From the determined potential, we have calculated local properties and have compared them with STS data. Figure 3(b) shows the differential conductance measured in the center of these four regions and Fig. 3(c) the corresponding LDOS spectra. The pronounced dip appearing close to the Fermi energy corresponds to the complete gap in the surface density of states. We would like to point out that the spectral intensity in the hcp region is significantly lower than in the three other regions for small energies (<0.1 eV) suggesting that the surface potential is high in the hcp triangles as obtained in our potential determination. Around 0.12 eV, the spectral intensity in the hcp region increases rapidly. This variation results from the third band at the $M$ point (Fig. 2). Finally, a dip in the fcc and hcp regions and protrusion in the side region appear around 0.35 eV. This behavior is related to the opening of the second gap at the $M$ point.

In Figs. 4(a) and 4(b), we compare differential conductance maps recorded at three characteristic energies and the corresponding calculated LDOS. The first energy (−70 meV) was chosen below the first gap at the maximum of the spectral peak, the second one (40 meV) is just above the gap, whereas the third one (360 meV) corresponds to the second gap at the $M$ point. Very good agreement is obtained between the experimental and calculated maps. Below the first gap, the maxima of the local density of states are located in the fcc1 regions, whereas they are in the fcc2 regions above this gap. At the energy of opening of the second gap at the $M$ point (350 meV), the electronic density is more structured and maxima appear in the side regions. The good agreement between measured and calculated conductance spectra (Fig. 3) and maps (Fig. 4) shows that the potential estimated from gap widths in ARPES describes remarkably the local properties.

In this Rapid Communication, we propose a methodological approach to obtain the surface potential from gaps associated with the nanostructurated surface of Ag/Cu(111). The determination of these energy band gaps by ARPES and symmetry arguments leads to an estimation of the first two Fourier components from which we can build an excellent approximation of the potential. Local properties such as the LDOS and surface band structure can be satisfactorily described by this potential. Such an original and simple approach could be used to model the electronic properties at the nanometric scale as soon as the nearly-free-electron model is a good approximation.

[1] L. Bürgi, H. Brune, and K. Kern, Phys. Rev. Lett. **89**, 176801 (2002).

[2] M. Tinkham, *Group Theory and Quantum Mechanics* (McGraw-Hill, New York, 1964).

[3] E. Starodub, A. Bostwick, L. Moreschini, S. Nie, F. E. Gabaly, K. F. McCarty, and E. Rotenberg, Phys. Rev. B **83**, 125428 (2011).

[4] D. Malterre, B. Kierren, Y. Fagot-Revurat, C. Didiot, F. J. García de Abajo, F. Schiller, J. Cordón, and J. E. Ortega, New J. Phys. **13**, 013026 (2011).

[5] F. Reinert, G. Nicolay, S. Schmidt, D. Ehm, and S. Hüfner, Phys. Rev. B **63**, 115415 (2001).

[6] A. Mugarza and J. E. Ortega, J. Phys.: Condens. Matter **15**, S3281 (2003).

[7] C. Didiot, Y. Fagot-Revurat, S. Pons, B. Kierren, C. Chatelain, and D. Malterre, Phys. Rev. B **74**, 081404(R) (2006).

[8] I. Meunier, G. Tréglia, J.-M. Gay, B. Aufray, and B. Legrand, Phys. Rev. B **59**, 10910 (1999).

[9] A. Bendounan, H. Cercellier, Y. Fagot-Revurat, B. Kierren, V. Y. Yurov, and D. Malterre, Phys. Rev. B **67**, 165412 (2003).

[10] F. Schiller, J. Cordón, D. Vyalikh, A. Rubio, and J. E. Ortega, Phys. Rev. Lett. **94**, 016103 (2005).

[11] A. Bendounan, F. Forster, J. Ziroff, F. Schmitt, and F. Reinert, Phys. Rev. B **72**, 075407 (2005).

[12] A. Bendounan, F. Forster, F. Reinert, B. Kierren, Y. Fagot-Revurat, and D. Malterre, Phys. Rev. Lett. **96**, 029701 (2006).

[13] See, for example, N. W. Ashcroft and N. D. Mermin, *Solid State Physics* (Brooks Cole, New York, 1976).

[14] Z. M. Abd El-Fattah, M. Matena, M. Corso, F. J. García de Abajo, F. Schiller, and J. E. Ortega, Phys. Rev. Lett. **107**, 066803 (2011).

[15] F. J. García de Abajo *et al*., Nanoscale **2**, 717 (2010).

[16] S. Achilli, M. I. Trioni, and E. V. Chulkov, Phys. Rev. B **85**, 045408 (2012).

[17] H. Bentmann, A. Buchter, and F. Reinert, Phys. Rev. B **85**, 121412 (2012).